Geochemistry Geophysics Geosystems G3

Article
Volume 13, Number 1
19 January 2012
Q0AD22, doi:10.1029/2011GC003782
ISSN: 1525-2027

Published by AGU and the Geochemical Society

Pliocene shortening direction in Nankai Trough off Kumano, southwest Japan, Sites IODP C0001 and C0002, Expedition 315: Anisotropy of magnetic susceptibility analysis for paleostress

Toshiya Kanamatsu
Institute for Research on Earth Evolution, Japan Agency for Marine-Earth Science and Technology, 2-15 Natsushima-cho, Yokosuka 237-0061, Japan (toshiyak@jamstec.go.jp)

Josep M. Parés
Department of Earth and Environmental Sciences, University of Michigan, Ann Arbor, Michigan 48109, USA

Now at CENIEH, Paseo Sierra de Atapuerca s/n, E-09002 Burgos, Spain

Yujin Kitamura
Institute for Research on Earth Evolution, Japan Agency for Marine-Earth Science and Technology, 2-15 Natsushima-cho, Yokosuka 237-0061, Japan

[1] Integrated Ocean Drilling Program Expedition 315 recovered cores from accretionary units, which are overlain by cover sequences, at a site on the hanging wall of the mega-splay fault (C0001), and at a seaward margin of a forearc basin (C0002) in Nankai Trough off Kumano, Japan. In order to investigate the amount and the style of deformation and shortening direction of the accretionary prism units, anisotropy of magnetic susceptibility (AMS) of cored samples were measured. AMS of the late Pliocene to late Miocene accretionary prism at C0001 reveals a deformed magnetic ellipsoid (prolate type), and a restored direction of the AMS orientation indicates northwest–southeast shortening which is the same as the present-day stress field measured by borehole breakout. The older Miocene accretionary prism cored beneath the forearc basin at C0002 does not show a typical prolate type but more oblate feature in parallel to plunged bedding planes. This type can be interpreted as an intermediate type between prolate and oblate types, by indicatives of AMS parameters, which was formed under a bedding vertical loading and a relatively weakly lateral compaction. The restored AMS orientation of the accretionary prism beneath the forearc basin also indicates the northwest-southeast shortening which is different from the present-day principal horizontal stress orientations at C0002. It is supposed that the shortening direction had been recorded in Pliocene time probably when the sequence was sited in the outer wedge. The northwest–southeast directions of AMS in the Pliocene time agree with the past subducting direction of the Philippine Sea Plate since the Pliocene.

Components: 6000 words, 8 figures.

Keywords: NanTroSEIZE; accretionary prism; anisotropy of magnetic susceptibility; subduction zone.

Index Terms: 1518 Geomagnetism and Paleomagnetism: Magnetic fabrics and anisotropy; 3036 Marine Geology and Geophysics: Ocean drilling; 8170 Tectonophysics: Subduction zone processes (1031, 3060, 3613, 8413).

Received 7 July 2011; **Revised** 30 November 2011; **Accepted** 30 November 2011; **Published** 19 January 2012.

Kanamatsu, T., J. M. Parés, and Y. Kitamura (2012), Pliocene shortening direction in Nankai Trough off Kumano, southwest Japan, Sites IODP C0001 and C0002, Expedition 315: Anisotropy of magnetic susceptibility analysis for paleostress, *Geochem. Geophys. Geosyst.*, *13*, Q0AD22, doi:10.1029/2011GC003782.

Theme: Mechanics, Deformation, and Hydrologic Processes at Subduction Complexes, with Emphasis on the NanTroSEIZE Drilling Transect

1. Introduction

[2] Multi drilling expeditions under the Integrated Ocean Drilling Program (IODP) were designed for the Nankai Trough Seismogenic Zone Experiment (NanTroSEIZE). The ultimate goal in NanTroSEIZE is to achieve sampling and monitoring of the great earthquake rupture zone off Kumano, Japan [*Tobin and Kinoshita*, 2006]. At the early stage of NanTroSEIZE, Expeditions 315, 316, 322, and 333 [*Ashi et al.*, 2009; *Screaton et al.*, 2009; *Saito et al.*, 2010; *Henry et al.*, 2010] cored the shallow portion of the Nankai accretionary wedge and the subduction input section in order to understand characteristics of material across the subduction zone widely. Coring by the different expeditions covered various tectonic settings, including the subduction input, the subduction front, the frontal thrust region, the shallow portion of the megasplay system, and the seaward margin of forearc basin across NanTroSEIZE study area.

[3] Besides the drilling campaign, detailed seismic reflection surveys imaged an outline of the accretionary wedge and fault systems developed in the NanTroSEIZE area [*Moore et al.*, 2007, 2009]. Images of accretionary sequences in various tectonic settings are revealed: accretionary prism in the frontal thrust region, imbricated accretionary sequences in the middle of outer wedge, further deformed accretionary sequences by a mega-splay fault system, a forearc high, and the Kumano Basin (Figure 1a). In such a deformation process, strain changes in accretionary sequences would occur progressively or dramatically. *Moore et al.* [2010] find that a significant amount of total horizontal shortening is proceed in outside of the outer wedge, and that porosity loss and associated dewatering decrease progressively landward.

[4] Measuring those changes across the subduction zone using samples obtained by the drilling facilitates our understanding of the tectonic development of accretionary wedges. We employed the anisotropy of magnetic susceptibility (AMS) method to detect strain in sediments. AMS allows distinguishing features in rock fabrics in response to tectonic domains which record the systematic reorientation of the original fabric. Previous works have demonstrated that AMS is an excellent strain indicator which sensitively reflects a local convergent tectonic environment [*Parés et al.*, 1999; *Owens*, 1993; *Ujiie et al.*, 2003; *Housen et al.*, 1996; *Housen and Kanamatsu*, 2003; *Hrouda et al.*, 2009; *Kitamura et al.*, 2010]. Encouraged by these existing results, we expect that AMS method will document effectively the deformation styles of sediment which provide useful information for understanding the material state change in the subduction zone. We intend to study the change of strain in the accretionary prism through time and space with AMS method.

2. Geological Background

[5] In IODP Expedition 315, accretionary prism units in two different local settings were recovered (Figure 1b). One is beneath a cover sediment in the upper slope (Site IODP C0001), and the other is beneath Kumano forearc basin deposit (Site IODP C0002) [*Ashi et al.*, 2009].

[6] Site C0001 is located in the hanging wall of the seaward-most branches of the mega-splay fault system [*Expedition 315 Scientists*, 2009a]. The slope basin sediments are approximately 200 m thick and overly the accretionary wedge by an unconformity (Figure 2). Recovered sediment in 0–207.17 m core depth below seafloor (CSF) reveals that the slope sediment (Unit C1U1) is composed of Quaternary to late Pliocene fine grain sediment with a number of tephra layers (Figure 2). Minor structures of conjugate normal faults, breccia and shear occurrence are documented. Although bedding dip is generally subhorizontal, several intervals reveal pronounced variable dips at 80–100, 140, and 200–205 m CSF. At the base of C1U1, a thick sand layer overlies the late Pliocene to late Miocene accretionary prism (Unit C1U2), which involves structures such as normal, thrust, and strike-slip faults. These structures seem to be developed in different stages. The dominant lithology of C1U2 is bioturbated mud (silty clay-clayey silt). Low concentra-

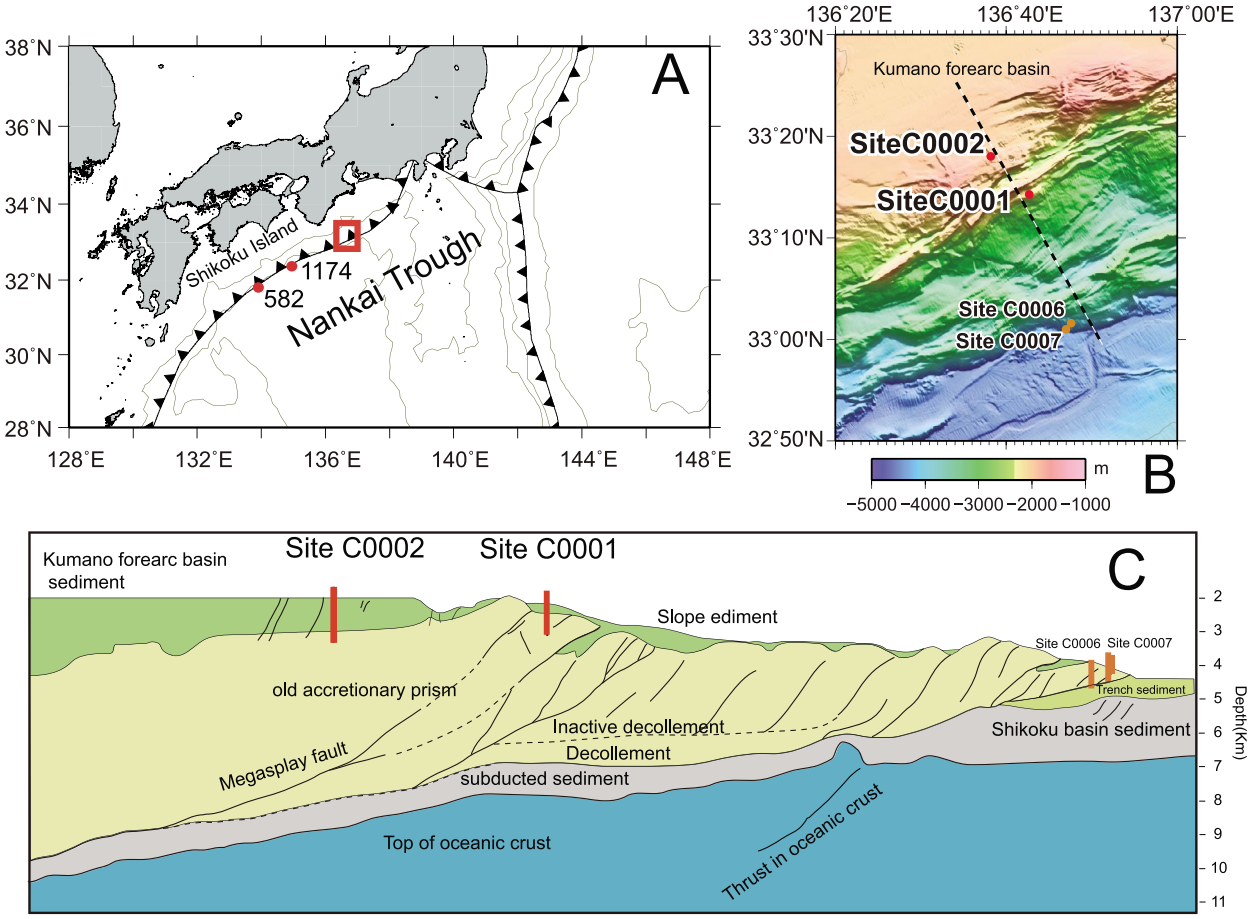

Figure 1. (a) NanTroSEIZE study area. DSDP site 582 and ODP site 1174 are also shown. (b) Location and bathymetry of the studied area. Coring sites for this study are plotted in red solid circles. (c) Interpreted seismic cross section of Nankai Trough, along NanTroSEIZE drilling sites simplified from [*Moore et al.*, 2009]. Coring sites for NanTroSEIZE stage 1 are shown.

tions of calcareous nanofossil in C1U2 point to a depositional environment below the carbonate compensation depth (CCD), suggesting near the base of the trench slope. Although muddy facies is not usual at trench-wedge environment, onboard preferred interpretation for the depositional environment is outer trench wedge during a time interval of low sand-silt influx [*Expedition 315 Scientists*, 2009a].

[7] Site C0002 is located at the southern margin of the Kumano forearc basin (Figure 1a). An approximately 920-m thick Kumano forearc basin sequence overlays an accretionary prism [*Expedition 315 Scientists*, 2009b]. Expedition 315 started coring at 475 m CSF, and recovered a forearc basin facies of ca 350-m thickness (the lower part of Unit II: C2U2) consisting of Quaternary fine grain sediment with occasionally interbedded sandy and volcanic ash layers (Figure 2). Subsequently a Pliocene basal forearc basin facies of ca 90-m thickness (Unit III: C2U3), which is characterized by a condensed mudstone section was cored. Beneath C2U3, ca. 130-m of the top of the Miocene (5.59–5.90 Ma) accretionary prism (Unit IV: C2U4) was cored. The lithofacies of C2U4, which is characterized by an alternation of fine grain and sandy facies, is distinguished by lithologic distribution from that of the overlying C2U3. The accretionary prism unit involves several kinds of deformation such as steepened bedding, faults, breccia, and shear zones. Three deformation stages were suggested by textures and crosscutting relations of structures [*Expedition 315 Scientists*, 2009b]. They are as follows: 1) The first phase of northwest–southeast shortening by thrust faulting and possibly strike-slip faulting, which is mainly accommodated in C2U4, 2) the second phase of northeast–southwest extension by normal faulting, and 3) the third phase

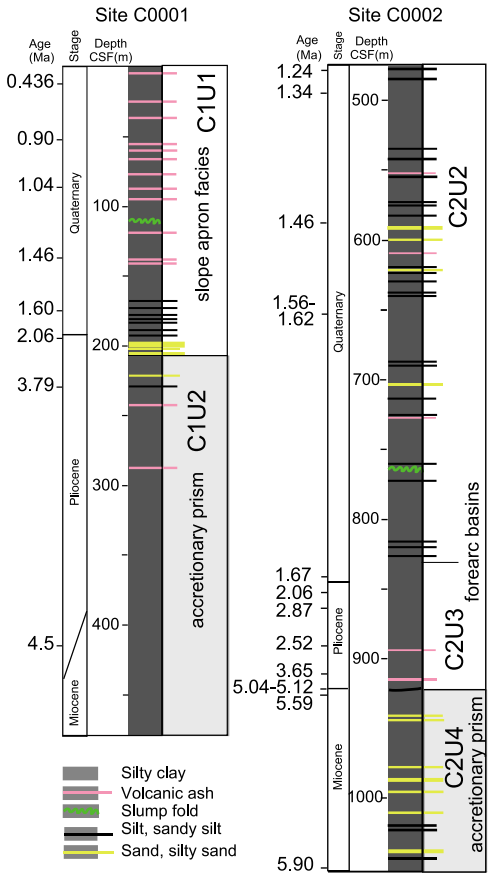

Figure 2. Lithology of sites C0001 and C0002, and their depositional ages from nanofossil datum. CSF: core depth below seafloor.

of north–south extension by normal faulting, showing a good correlation with borehole breakouts observed with LWD.

[8] As well as C1U2, low concentrations of calcareous nanofossils were observed, then the base of the trench slope is most likely depositional environment of C2U4. Although poor core recovery and a strong tectonic overprint make interpretation difficult, the lithofacies of C2U4 is interpreted as a boundary between accreted trench turbidites and muddy slope-apron deposits.

[9] Present-day principal horizontal stress states in the study area analyzed by borehole breakouts show that the stress distribution across the accretionary prism is not uniform [*Lin et al.*, 2010]. A contrasting difference in stress condition between Sites C0001 and C0002 is found in spite of a close distance (ca 10 km) between both sites. It indicates the orientation of the horizontal maximum principal stress is northwest–southeast for Site C0001 and northeast–southwest for Site C0002, respectively [*Kinoshita et al.*, 2009]. Strains in the accretionary prism are assumed to reflect such local stress fields.

3. Method

3.1. AMS

[10] AMS provides two types of information that characterize the rock fabric. One is the directional information represented by the orientations of three principal susceptibility axes that define the magnetic ellipsoid. In this paper we use the following terms to express the three principal axes; K1: maximum susceptibility, K2: intermediate susceptibility, and K3: minimum susceptibility. The second is the eccentricity of the anisotropy ellipsoid, which is defined by the relative magnitudes of the principal susceptibility axes and gives the degree of anisotropy. Anisotropy parameters calculated from measured data were used to express each eccentricity of magnetic ellipsoid. The following parameters were used to quantify the shape of the magnetic ellipsoids: P′ representing anisotropy degree, and T representing shape parameter were calculated from three principal axes.

$$P' = \exp\left(\sqrt{\left\{2\left[(\eta_1-\eta_m)^2+(\eta_2-\eta_m)^2+(\eta_3-\eta_m)^2\right]\right\}}\right),$$

$$T = \left[\frac{2(\eta_2-\eta_3)}{(\eta_1-\eta_3)}\right] - 1$$

Where η_1 = ln K1, η_2 = ln K2, η_3 = ln K3, and η_m = $(\eta_1 + \eta_2 + \eta_3)/3$. [*Jelinek*, 1981].

[11] In theory, AMS of sediment in an accretionary wedge will develop in three stages: settling of grains on the seafloor, subsequent sedimentary compaction, and tectonic compaction stages [e.g., *Parés et al.*, 1999; *Parés*, 2004]. During deposition and sedimentary compaction, grains with a shape anisotropy tend to preferentially fall with their K3 axes perpendicular to the depositional plane [e.g., *Tauxe*, 1998]. Consequently the magnetic fabric expresses an oblate shape (well-developed foliation). Because of shortening during the accretionary process, AMS will change to reflect a tectonic compaction fabric [e.g., *Housen et al.*, 1996; *Hrouda et al.*, 2009].

3.2. Magnetic Measurements

[12] A total of 366 samples were collected from Holes C0001 and C0002. Samples were taken from the center of the halved core to avoid drilling disturbance around the core liner or contamination form the walls. Layers containing deformation

structures such as faults and joints were avoided because they tend to reflect their local deformation. AMS was measured using an anisotropy of magnetic susceptibility measurement apparatus (Kappabridge KLY-4 AGICO Inc). In order to characterize the obtained AMS ellipsoids, we used the parametric bootstrapping method [*Tauxe*, 1998]. The method selects a number of data randomly and calculates means repeatedly. Bootstrapped principal magnetic susceptibility directions instead of an uncertainty ellipse are plotted to show a directional distribution. Additionally cumulative distributions of the bootstrapped values of principal normalized magnetic susceptibilities of K1, K2 and K3, are shown with the 95% confidence bounds to characterize magnetic ellipsoids. Measurements of magnetization were made using a horizontal 2-G cryogenic magnetometer (2-G Enterprises). Natural remanent magnetization (NRM) and demagnetization were routinely measured at several alternating field levels. Saturation isothermal remanent magnetization (SIRM) and thermal changes of magnetic susceptibility were measured on representative samples from each lithologic unit using Kappabridge KLY-4 attached to a CS3 apparatus (AGICO) in Ar atmosphere to identify the magnetic minerals in samples. All analyses were carried out at the Institute for Research on Earth Evolution, Japan Agency for Marine-Earth Science and Technology, Yokosuka Japan.

3.3. Core Orientation

[13] In order to investigate AMS directional distribution of each unit, we applied three different methods to restore core coordinates to geographic coordinates. When bedding plane is horizontal, paleomagnetic declinations were used to reorient AMS directions. For cores obtained by the hydraulic piston coring system (HPCS), the section-mean declinations (1.5 m-length generally) were calculated to have a sufficiently long time interval for averaging out geomagnetic secular variation. Cores sampled by the rotary core barrel (RCB) are generally broken into short pieces. Consequently those pieces have no consistent horizontal orientation within a section. For RCB samples, paleomagnetic declination of each sample was used to restore horizontal direction. For samples obtained from steeply inclined bedding interval, paleomagnetic declination cannot be simply applied for horizontal restoring. Instead we restored sample coordinates horizontally using X-ray computed tomography (X-ray CT) image of cores and resistivity borehole images. When a sedimentary sequence reveals a monocline structure, dip direction is uniquely defined. Dip directions of bedding structure in sampled pieces were analyzed by X-ray CT image using the software "OsiriX." Those directions of X-ray CT images were fitted to a predominant dip direction of the borehole image obtained by a logging-while-drilling (LWD) measurement at Site C0002 [*Expedition 314 Scientists*, 2009]. Using this procedure consequently 10 samples of C2U4 were successfully reconstructed.

4. Results

4.1. Magnetic Mineralogy

[14] We conducted several experiments to identify magnetic carriers. Isothermal remanent magnetization (IRM) acquisition curves were produced on selected samples (Figure 3a). Results show that IRMs are almost saturated around 300 mT, which indicates a ferrimagnetic mineral contribution, most likely magnetite as the remanent magnetization carrier. Mean S ratio [*Bloemendal et al.*, 1992] of the samples are 0.95, suggesting the presence of magnetite. The measurement of magnetic susceptibility while heating and cooling is carried out to estimate carrier of magnetic susceptibility. Typical results are shown in Figures 3b and 3c. A gradual decrease in magnetic susceptibility versus temperature from room temperature to 200°C is considered to be caused by the paramagnetic contribution, according to Curie-Weiss Law [e.g., *Hrouda et al.*, 1997] (Figures 3b and 3c). Most magnetic susceptibility curves increase at 300–500°C (Figures 3b and 3c). These patterns suggest the formation of a new magnetic mineral phase during the experiments. This phenomenon is probably due to a decomposition of iron sulfide or Fe-rich clay minerals and conversion to magnetite. A drop around 500–580°C is interpreted as the signature of the Curie temperature of magnetite. This magnetite is supposed to be originated from a mixture of initially existing and newly formed during experiment. During cooling procedures, magnetic susceptibility reaches a level of several times of magnetic susceptibility during heating, which also suggests new magnetite production by experiments. Only sample from C2U2 shows a different behavior. It shows a large increase of magnetic susceptibility during heating (Figure 3d), which is interpreted as a relatively large amount constituent of iron sulfide. A possible explanation of the difference is a different sedimentary environment of C2U2 relative to the other units (e.g., much

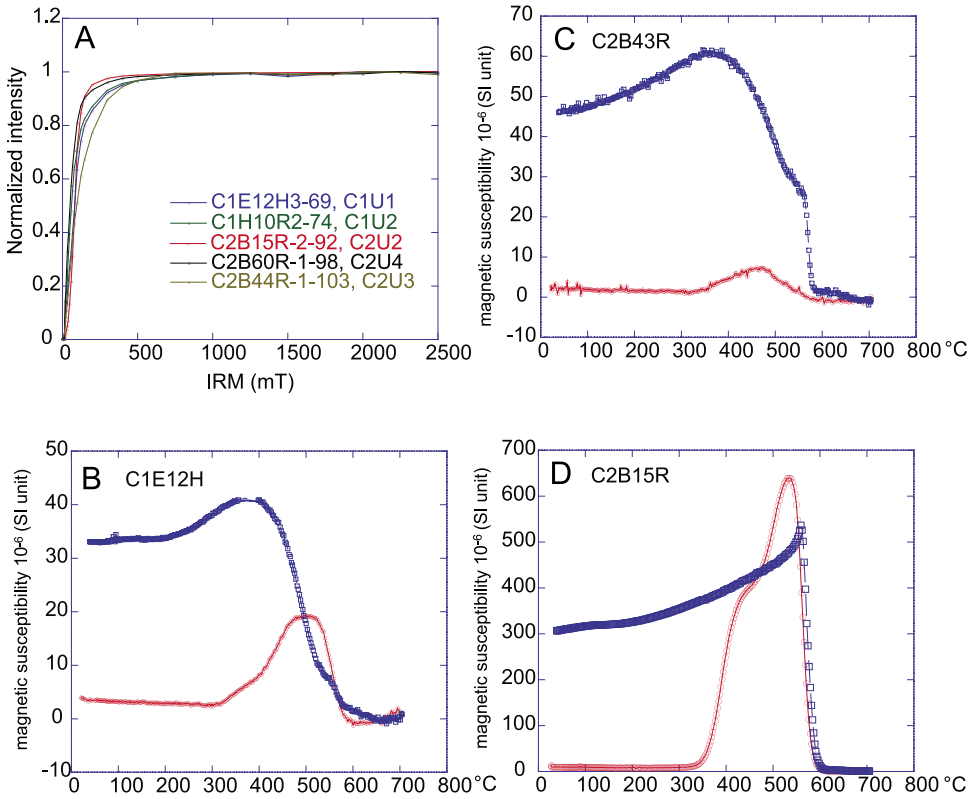

Figure 3. (a) Stepwise IRM acquisition experiments on C1U1, C1U2, C2U2, C2U3, and C2U4 samples. (b and c) Low-field magnetic susceptibility versus temperature dependencies for representatives from C1U1 (C1E12H) and C2U3 (C2B43R) sample, during heating (red) and cooling (blue) procedures. (d) Low-field magnetic susceptibility versus temperature dependencies for C2U2 (C2B15R) during heating (red) and cooling (blue) procedures.

reduction condition), although we have no independent data support it. Averaged magnetic susceptibility for C0001 and C0002 is weak, around 1.8×10^{-4}, and 2.5×10^{-4} (SI units) respectively. When a magnetic susceptibility of sample is low (ca. less than 5×10^{-4} SI unit), a significant paramagnetic contribution to the susceptibility and anisotropy is conceivable [*Tarling and Hrouda*, 1993]. These results do not identify definitely the carrier of magnetic susceptibility of the samples, but suggest that the existence of magnetite, iron sulfide, and paramagnetic clay minerals, and mixtures of them are possible contributors to magnetic susceptibility. Because we observe a similar magnetic mineralogical behavior of C1U1, C1U2, C2U3, and C2U4, we consider that the origin of magnetic susceptibility of each unit is rather similar, and will not consider that the difference in magnetic mineralogy is attributable to a difference in each AMS property except C2U2.

4.2. Down-Core AMS Parameters

[15] Generally, the anisotropy degree P′ increases downward through unit C1U1 (Figure 4a), a pattern that can be interpreted as foliated magnetic fabric developing with depth due to compaction. P′ suddenly drops just below the boundary between C1U1 and C1U2 units and then it shows a relatively constant value through C1U2, although some higher values are observed in a few tens meter below the unit boundary. The anisotropy shape factor T in C1U1 is dominantly positive, showing oblate type, while T values in C1U2 are scattered and dominantly negative compared to C1U1, showing prolate shape (Figure 4c). K3 inclinations are generally vertical in C1U1 (Figure 4c), but some shallower K3 inclination zones are observed. Shallow K3 axes in intervals of 80–140 and 194–207 m CSF are correlated to the variable bedding intervals at 80–100, 140, and 200–205 m [*Expedition 315 Scientists*, 2009a]. On the contrary, and regardless of horizontal bedding of C1U2 (Figure 4e), K3 axes inclination scatters through the entire interval (Figure 4d). Such pattern of AMS parameters and K3 inclinations through unit C1U2 suggest that the magnetic fabric is not a foliated magnetic fabric like observed in C1U1 unit. Because the magnetic parameters P′ and T show no significant changes

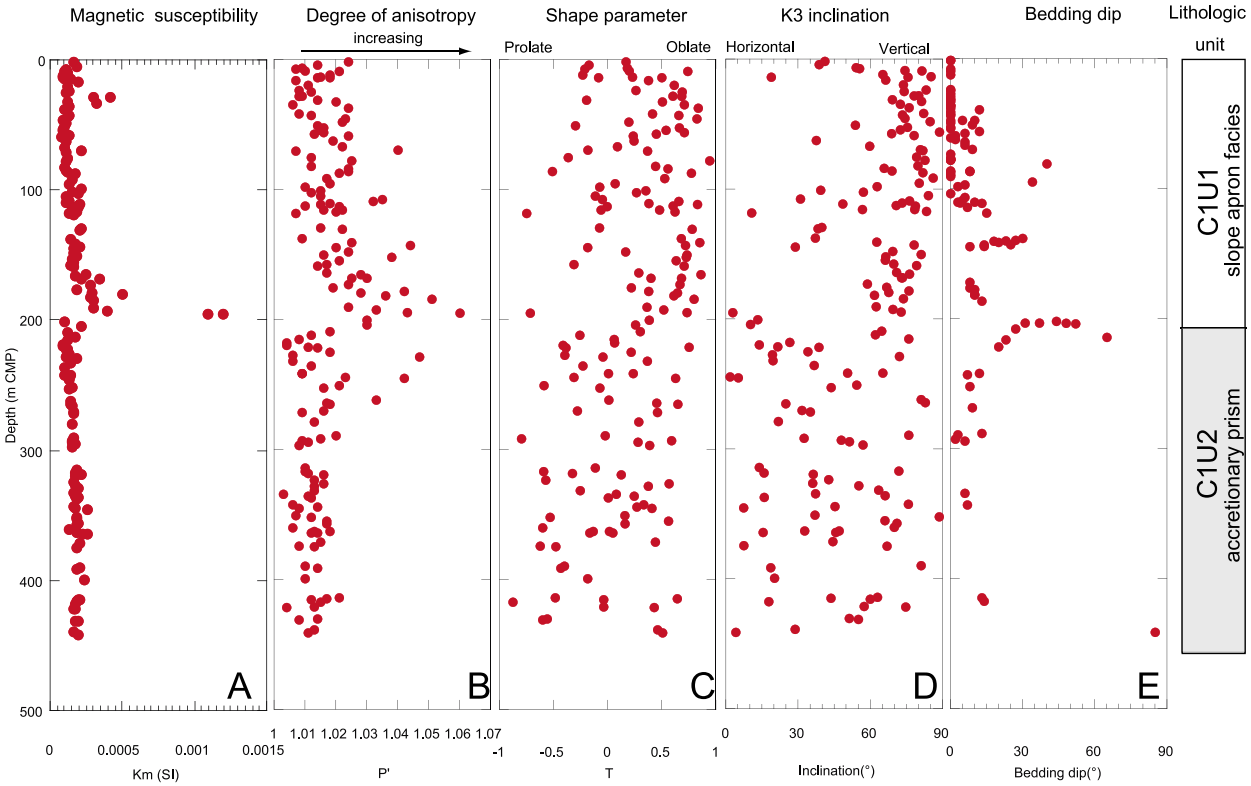

Figure 4. Down-core profiles of AMS parameters of Site C0001: (a) magnetic susceptibility, (b) degree of anisotropy (P′), (c) shape parameter (T), (d) K3 inclination, and (e) bedding dip in C0001 [*Expedition 315 Scientists*, 2009a].

through C1U2 unit (Figures 4b, 4c, and 4d), probably, the strain state in the unit is homogenous.

[16] Down-core P′ values at Site C0002 are relative constant throughout C2U2, C2U3 and C2U4 (Figure 5b). On the other side, a gradual decrease of T downward is recognized in the interval of C2U4 indicating that prolate type is more abundant in C2U4 than in C2U3 (Figure 5c). Down-core K3 inclination indicates a changing trend with the bedding dips (Figures 5d and 5e). This trend suggests that a direction of K3 inclination is strongly controlled by bedding plane.

4.3. AMS Orientation

[17] For cores of C1U1 recovered by HPCS, section-mean paleomagnetic declinations after AF cleaning at 30 mT were used for reorientation. We excluded data from samples in the intervals of abnormal bedding. Restored directions of C1U1 (Figure 6a) show that K3 axes are generally vertical, K1 and K2 are mostly scattered within the equatorial plane. For C1U2 recovered by RCB, paleomagnetic directions of each sample are used (Figure 6b). It shows systematic directions, which form a girdle of K3 and K2 around K1 axes. K1 axes dominantly align in northeast-southwest direction.

[18] Because C2U2 shows a different magnetic mineralogy, it has been excluded in this study. As bedding planes of C2U3 are generally gentle, paleomagnetic directions are used for re-orientation of AMS axes directions using the same method as for C1U2. K1 and K2 are mostly scattered within the equatorial plane with vertical K3 axis inclinations. K3 inclinations of C2U3 reveal magnetic foliation virtually horizontal (Figures 6c). Because bedding plans of C2U4 are significantly inclined (Figure 5e), the AMS directions of C2U4 were reoriented as described in section 3.3. Interpretations of borehole features in Hole C0002A, as derived from resistivity images in Hole C0002B [*Expedition 314 Scientists*, 2009], indicates that beds in the interval of C2U4 (921.73–1052.50 m CSF) dip southeastward dominantly. AMS axes of C2U4 were restored by fitting dip directions obtained from X-ray CT images to southeast (ca. 135°). After restoration, K3 directions are clustered around a northwest direction with steep

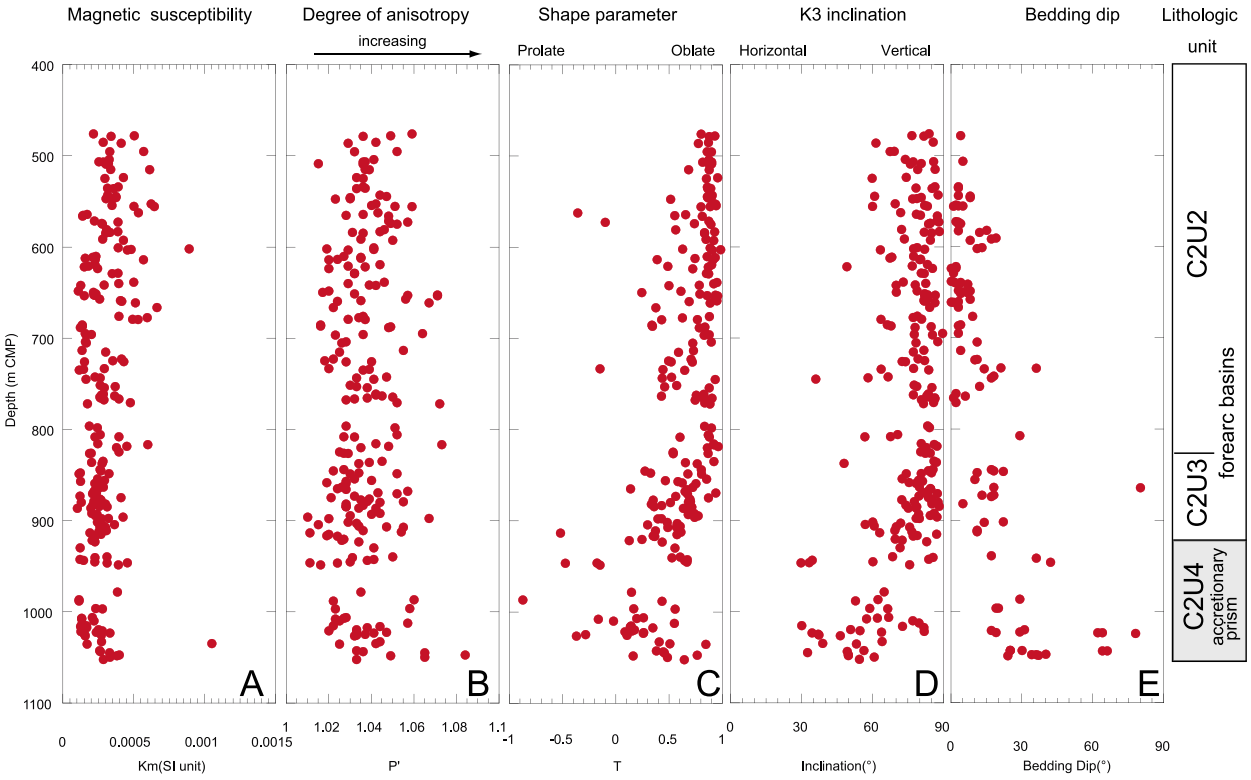

Figure 5. Down-core profiles of AMS parameters of Site C0002: (a) magnetic susceptibility, (b) degree of anisotropy (P′), (c) shape parameter (T), (d) K3 inclination, and (e) bedding dip in C0002 [*Expedition 315 Scientists*, 2009b].

inclinations. K1 directions scatter around a NE–SW direction (Figure 6d). K2 axes are scattered around a southeast direction and have shallow inclinations.

4.4. AMS Ellipsoid

[19] Directions of C1U1 and C2U3 show that K3 bootstrapped eigenvectors are well defined, and K1

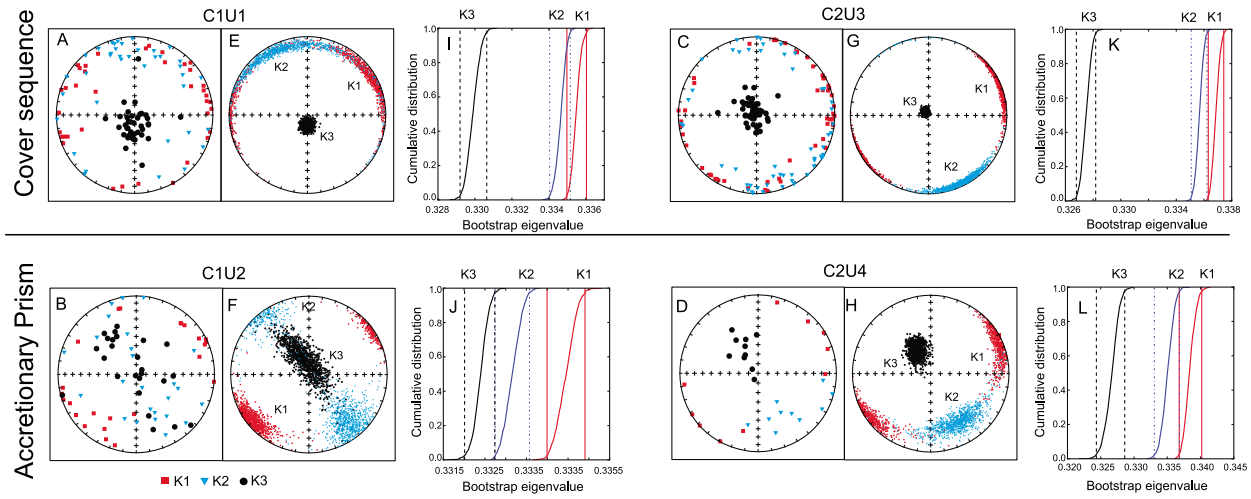

Figure 6. AMS directions and distributions of normalized magnetic susceptibility values for units in sites C0001 and C0002. (a–d) K1 (red), K2 (blue) and K3 (black) principal magnetic susceptibility directions projected on lower-hemisphere in equal-area projection. (e–h) Bootstrapped K1, K2 and K3, directions projected on lower-hemisphere in equal-area projection. (i–l) Cumulative distributions of bootstrapped normalized magnetic susceptibility values, K1, K2 and K3, shown with the 95% confidence bounds. Parts of Figure 6 were prepared with L. Tauxe's PmagPy-2.51 software package.

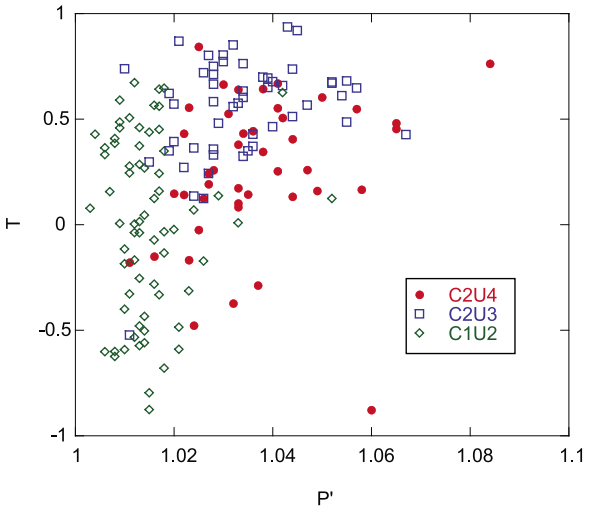

Figure 7. T and P′ magnetic parameter distribution of magnetic fabric parameters of C2U4 with C2U3 and C1U2.

and K2 of each unit form a girdle with a wider distribution in the equatorial plane (Figures 6e and 6g), and 95% confidence bound of K3 bootstrapped eigenvalues is distinct from those of K1 and K2 for both units (Figures 6e and 6k). Accordingly AMS ellipsoids of C1U1 and C2U3 are categorized to oblate patterns. In contrast, bootstrap directions of eigenvectors of C1U2 show a girdle of K3 and K2 axes around K1 axes (Figure 6f). 95% confidence bound of K1 is distinct, and K2 and K3 occur side-by-side (Figure 6j). This pattern characterizes as a prolate type ellipsoid. The distribution of C2U4 eigenvector indicates oblate ellipsoids (Figure 6h), which shows a distinct K3 distribution. The bound of confidence intervals of eigenvalues K3 is not distinct from those in C1U1 and C2U3, but ranges near to bounds of K1 and K2 like C1U2 (Figure 6l). This eigenvalue distribution indicates a less oblate ellipsoid, which K3 does not stand out so much from K1 and K2. These observations suggest that C2U4 sediments have typically very low eccentricity ellipsoids. Such ellipsoids could be categorized to a weak triaxial as described by *Schwehr and Tauxe*, [2003]. T-P′ diagram [*Jelinek*, 1981] is shown to compare magnetic ellipsoid of C2U4 with C1U2 (prolate) and C2U3 (oblate) in Figure 7. C2U4 distribution, which occupies an intermediate area

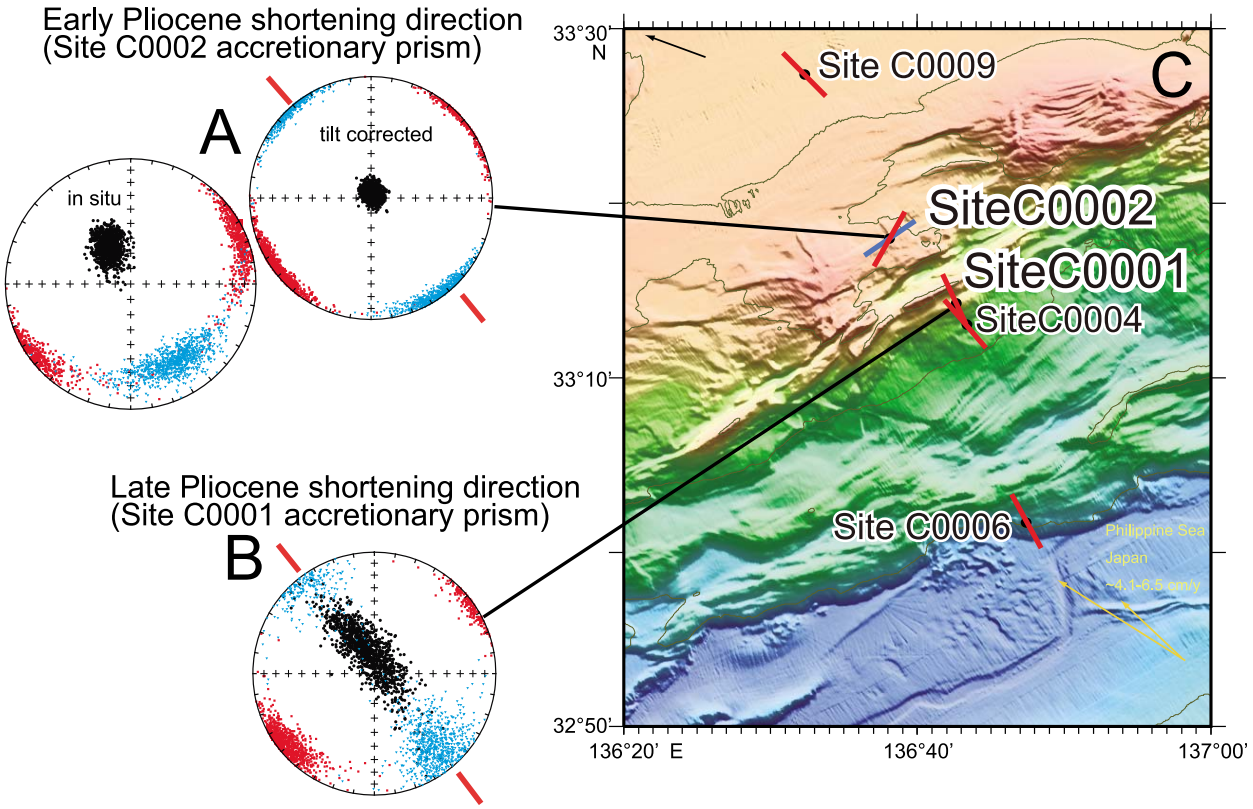

Figure 8. Shortening direction of accretionary prism of (a) C0001 and (b) C0002 inferred from AMS (red line). (c) Orientation of horizontal maximum stress fields determined from borehole breakouts [*Expedition 319 Scientists*, 2010].

between both, ensures that C2U4 ellipsoid is an intermediate type between oblate and prolate.

5. Discussion

[20] Within an accretionary wedge, prolate magnetic ellipsoids such as those observed in C1U2 unit have been often reported [e.g., *Hrouda et al.*, 2009]. This type of ellipsoids is interpreted as a result of layer parallel shortening caused by an accretionary process. Thus we consider that C1U2 magnetic fabric was also formed by a similar process. In such magnetic fabric, the shortening direction is always perpendicular to K1 axes direction. The mean direction of K1 axes of C1U2 is 232.7°, and therefore the inferred horizontal shortening would have a northwest-southeast direction (Figure 8b). The original depositional setting of C1U2 unit was around the trench wedge prior to the laterally being compacted by the accretionary process. The possible oldest timing of locking AMS, therefore, is after the sedimentation of C1U2. On the other hand, because AMS of C1U1, which overlies C1U2 with the unconformity, does not show such a shortening signature, the inferred lateral shortening could have taken place before the onset of sedimentation of C1U1. Ages of the top of C1U2 and the base of C1U1 are estimated as 3.79 Ma, and ~2 Ma, respectively. It is, therefore, surmised that this lateral shortening occurred at some time between ~2 Ma and 3.79 Ma (late Pliocene). The current stress direction inferred from the borehole breakout at C0001 [*Kinoshita et al.*, 2009] has a similar direction to the inferred from AMS. Thus, it is proposed that a similar tectonic context as in the present-day formed C1U2 AMS ellipsoid.

[21] AMS of C2U4 accretionary prism reveals an oblate-like feature. However, the detailed comparison of AMS parameters among the units reveals that C2U4 has an intermediate type between oblate and prolate ellipsoids (Figure 7). In order to understand the origin of the magnetic fabric further, the relationship between bedding attitude and orientation of magnetic axes are examined. AMS axes directions of C2U4 have been restored into the tilt-adjusted coordinate system (Figure 8a tilt-corrected). After tilt-corrections, K3 axes are more clustered, indicating that the magnetic fabric was formed when bedding planes were horizontal (K3: zeta/eta 17.6/12.3 in situ and 14.1/11.1 after tilt-correction). It therefore possible that K1 axes alignment reflects the sediment transport direction as described in section 3.1. The depositional environment of C2U4 is thought to occur around the trench wedge [*Expedition 315 Scientists*, 2009b]. In such conditions, the magnetic fabric is expected to be formed by a bottom current along a trench axis. In fact *Taira and Niitsuma* [1986] found oblate magnetic fabrics with K1 axes aligned by turbidity currents in the trench at DSDP Site 582 (Figure 1a) in Nankai Trough off Ashizuri. The initial magnetic fabric of C2U4 is assumed to have been similar to that of Site 582. But shape parameters of C2U4 indicate more prolate fabric, implying an overprint on the initial magnetic fabric by a tectonic deformation. A magnetic fabric in the accretionary prism above the decollement zone at ODP site 1174 (Figure 1a), Nankai Trough off Muroto seems to be an analog of C2U4 magnetic fabric. *Ujiie et al.* [2003] regarded that the magnetic fabric was formed by an initial bedding parallel compaction and then modified with a lateral compression driven by plate convergence at the accretionary prism toe. As a consequence of this lateral shortening, K1 axis moves into a perpendicular direction to the lateral compressional direction. The magnetic fabric of C2U4 seems to record such shortening during the initial stages of accretion in the outer wedge.

[22] Onboard independent structure analysis on C2U4 indicates that a lateral northwest-southeast shortening occurred in the early phase of the deformation history of C2U4 [*Expedition 315 Scientists*, 2009b]. Because K1 northeast-southwest directions of C2U4 are perpendicular to this shortening direction, the shortening event probably changed the magnetic fabric and accounts for the K1 orientation indicating northwest-southeast. All together, it seems that K1 orientation of C2U4 has been formed under a lateral shortening during the accretionary process.

[23] The present horizontal maximum principal stress orientation inferred from an analysis of borehole breakouts [*Lin et al.*, 2010], and anelastic strain recovery at C0002 [*Byrne et al.*, 2009] shows northeast-southwest trend, which is orthogonal to the AMS shortening direction. The different direction of AMS from the present stress-field implies that AMS had been locked as a strain gauge when the thrust sheet was in the outer wedge, and has not been influenced by the present stress field in the southern margin of Kumano basin. The timing of locking AMS is estimated to occur some time after the deposition of C2U4 (5.04–5.12 Ma), and before the start of deposition of C2U3 (3.65 Ma), early Pliocene, following the same reasoning as in unit C1U2.

[24] AMS analysis from the lower part of the wedge at the accretionary front at sites C0006 and

C0007 (Figure 1), in the NanTroSEIZE transect [*Kitamura et al.*, 2010; *Byrne et al.*, 2009] indicate that the magnetic fabric in the lower part of accreted sediment is characterized by shallow of K3 axes. Such inclinations are interpreted as a result of strong horizontal compression caused by a sediment underplating in the accretionary front. These authors interpreted that horizontal strain become strong downward at the prism toe. AMS ellipsoids of C1U2 and C2U4 do not show shallow K3 inclinations as those of AMS at the prism toe. This indicates the weaker laterally compacted ellipsoids of C1U2 and C2U4 compared to C0006 and C0007.

[25] Several papers discuss stress regimes in the Kumano wedges in space and time. *Gulick et al.* [2010] demonstrated the tectonic history of southwest of the Kumano Basin in the early Quaternary by analyzing of 3-D seismic images. An extensive landward tilting of the outer Kumano Basin is found in the middle to late Quaternary (1.3–1.0 Ma). This event could be related to a major active phase of the mega-splay fault revealed by *Strasser et al.* [2009]. *Gulick et al.* [2010] then suggests the extensive shortening of the entire wedges happened within the limited period. This temporal stress variation could make different deformation records on magnetic fabrics in the accretionary wedge. Our interpretation on the contrasting magnetic fabrics between C1U2 and C2U4 is that shortening occurs at different times in the Kumano accretionary wedge. Parameters of C2U4 suggest the weaker shortening than that of C1U2 (Figure 7). One of the factors, which control the shortening of outer wedge, is probably the subduction velocity of Philippine Sea Plate. *Kimura et al.* [2005] propose the slower subduction rate of Philippine Sea Plate as 0.9 cm/yr during 12–4 Ma, and the higher rate, in turn, as 4 cm/yr during 4–0 Ma by the interpretation of space-time evolution of subduction-related igneous activity in southwest Japan. The lower convergent rate at Kumano Trough perhaps accounts for the weaker deformation of C2U4 in some time during 3.65–5.12 Ma.

[26] Magnetic fabrics in C1U2 and C2U4 reveal northwest-southeast shortening directions in Pliocene times (2–3.79Ma to 3.65–5.54 Ma). These shortening directions are concordant with the current horizontal compression direction induced by plate convergence. According to *Yoshioka and Murakami* [2007], the relative plate motion of the subducting Philippine Sea Plate at the trench have been northwestward since 5Ma. So that a convergent direction at the toe of accretionary prism is expected in northwest-southeast for that time. Shortening directions inferred by AMS is consistent with the past subducting direction of the Philippine Sea Plate. Thus we regard AMS directions at C0001 and C0002 as archives of paleo-stress field proxies for a northwest-southeast horizontal compression active during plate subduction.

6. Conclusion

[27] AMS of the accretionary prism cored during IODP Expedition 315 in the mega-splay fault zone, and beneath the forearc basin has been studied. AMS of cover sequences in both sites show oblate ellipsoids with vertical K3 axes, normal to bedding plane, which formed by vertical loading.

[28] AMS ellipsoids of the Pliocene accretionary prism cored at C0001 in the upper slope, reveal prolate type ellipsoids, which are characterized by a girdle of K2 and K3 axes around K1 axes. Reoriented AMS axis directions indicate a northwest-southeast shortening direction. This shortening occurred sometime between 2 and 3.79 Ma (late Pliocene). On the other hand, AMS ellipsoids of accretionary prism beneath the Kumano forearc basin at C0002 is interpreted as weakly deformed ellipsoids produced under a vertical compaction and a relatively weak horizontal shortening. K1 axes are perpendicular to the northwest-southeast lateral shortening. The AMS fabric is interpreted to have been locked before tilting and during the time interval of 3.65 to 5.04–5.12 Ma (early Pliocene). Both directions shortening in the accretionary prism units are consistent with the subducting plate direction of the Philippine Sea plate since Pliocene.

Acknowledgments

[29] We would like to thank our IODP NanTroSEIZE Expeditions stage 1 colleagues for encouraging discussion and useful suggestions related to this work. We greatly thank the reviews by Bernard Housen and an anonymous reviewer, who significantly improved the manuscript. This study used samples and data provided by the Integrated Ocean Drilling Program (IODP). This work was partially supported by KAKENHI 19GS0211 and 21107001. Figure 6 was prepared with L. Tauxe's PmagPy-2.51 software package.

References

Ashi, J., S. Lallemant, H. Masago, and the Expedition 315 Scientists (2009), Expedition 315 summary, *Proc. Integr. Ocean Drill. Program*, *314/315/316*, 34 pp., doi:10.2204/iodp.proc.314315316.121.2009.

Bloemendal, J., J. W. King, F. R. Hall, and S.-J. Doh (1992), Rock magnetism of Late Neogene and Pleistocene deep-sea sediments: Relationship to sediment source, diagenetic processes, and sediment lithology, *J. Geophys. Res.*, *97*, 4361–4375, doi:10.1029/91JB03068.

Byrne, T. B., W. Lin, A. Tsutsumi, Y. Yamamoto, J. C. Lewis, K. Kanagawa, Y. Kitamura, A. Yamaguchi, and G. Kimura (2009), Anelastic strain recovery reveals extension across SW Japan subduction zone, *Geophys. Res. Lett.*, *36*, L23310, doi:10.1029/2009GL040749.

Expedition 314 Scientists (2009), Expedition 314 Site C0002, *Proc. Integr. Ocean Drill. Program*, *314/315/316*, 77 pp., doi:10.2204/iodp.proc.314315316.114.2009.

Expedition 315 Scientists (2009a), Expedition 315 Site C0001, *Proc. Integr. Ocean Drill. Program*, *314/315/316*, 104 pp., doi:10.2204/iodp.proc.314315316.123.2009.

Expedition 315 Scientists (2009b), Expedition 315 Site C0002, *Proc. Integr. Ocean Drill. Program*, *314/315/316*, 76 pp., doi:10.2204/iodp.proc.314315316.124.2009.

Expedition 319 Scientists (2010), Site C0009, *Proc. Integr. Ocean Drill. Program*, *319*, 180 pp., doi:10.2204/iodp.proc.319.103.2010.

Gulick, S. P. S., et al. (2010), Rapid forearc basin uplift and megasplay fault development from 3D seismic images of Nankai margin off Kii Peninsula, Japan, *Earth Planet. Sci. Lett.*, *300*, 55–62, doi:10.1016/j.epsl.2010.09.034.

Henry, P., T. Kanamatsu, and K. T. Moe (2010), NanTroSEIZE Stage 2: Subduction inputs 2 and heat flow, *Integr. Ocean Drill. Program Sci. Prosp.*, *333*, 55 pp.

Housen, B.A., and T. Kanamatsu (2003), Magnetic fabrics from the Costa Rica margin: Sediment deformation during the initial dewatering and underplating process, *Earth Planet. Sci. Lett.*, *206*, 215–228, doi:10.1016/S0012-821X(02)01076-2.

Housen, B. A., H. J. Tobin, P. Labaume, E. C. Leitch, and A. J. Maltman, and the Ocean Drilling Program Leg 156 Shipboard Science Party (1996), Strain decoupling across the decollement of the Barbados accretionary prism, *Geology*, *24*, 127–130, doi:10.1130/0091-7613(1996)024<0127:SDATDO>2.3.CO;2.

Hrouda, F., V. Jelínek, and K. Zapletal (1997), Refined technique for susceptibility resolution into ferromagnetic and paramagnetic components based on susceptibility temperature-variation measurement, *Geophys. J. Int.*, *129*, 715–719, doi:10.1111/j.1365-246X.1997.tb04506.x.

Hrouda, F., O. Krejčíc, M. Potfajd, and Z. Stráník (2009), Magnetic fabric and weak deformation in sandstones of accretionary prisms of the Flysch and Klippen Belts of the Western Carpathians: Mostly offscraping indicated, *Tectonophysics*, *479*, 254–270, doi:10.1016/j.tecto.2009.08.016.

Jelinek, V. (1981), Characterization of the magnetic fabric of rocks, *Tectonophysics*, *79*, T63–T67, doi:10.1016/0040-1951(81)90110-4.

Kimura, J., R. J. Stern, and T. Yoshida (2005), Reinitiation of subduction and magmatic responses in SW Japan during Neogene time, *Geol. Soc. Am. Bull.*, *117*, 969–986, doi:10.1130/B25565.1.

Kinoshita, M., H. Tobin, J. Ashi, G. Kimura, S. Lallemant, E. J. Screaton, D. Curewitz, H. Masago, K. T. Moe, and the Expedition 314/315/316 Scientists (2009), *Proceedings of the Integrated Ocean Drilling Program*, vol. 314/315/316, Integr. Ocean Drill. Program Manage. Int., Inc., Washington, D. C.

Kitamura, Y., T. Kanamatsu, and X. Zhao (2010), Structural evolution in accretionary prism toe revealed by magnetic fabric analysis from IODP NanTroSEIZE Expedition 316, *Earth Planet. Sci. Lett.*, *292*, 221–230, doi:10.1016/j.epsl.2010.01.040.

Lin, W., et al. (2010), Present-day principal horizontal stress orientations in the Kumano forearc basin of the southwest Japan subduction zone determined from IODP NanTroSEIZE drilling Site C0009, *Geophys. Res. Lett.*, *37*, L13303, doi:10.1029/2010GL043158.

Moore, G. F., N. L. Bangs, A. Taira, S. Kuramoto, E. Pangborn, and H. J. Tobin (2007), Three-dimensional splay fault geometry and implications for tsunami generation, *Science*, *318*, 1128–1131, doi:10.1126/science.1147195.

Moore, G. F., et al. (2009), Structural and seismic stratigraphic framework of the NanTroSEIZE Stage 1 transect, *Proc. Integr. Ocean Drill. Program*, *314/315/316*, doi:10.2204/iodp.proc.314315316.102.2009.

Moore, G. F., D. Saffer, M. Studer, and P. Costa Pisani (2010), Structural restoration of thrusts at the toe of the Nankai Trough accretionary prism off Shikoku Island, Japan: Implications for dewatering processes, *Geochem. Geophys. Geosyst.*, *12*, Q0AD12, doi:10.1029/2010GC003453.

Owens, W. (1993), Magnetic fabric studies of samples from Hole 808C, Nankai Trough, *Proc. Ocean Drill. Program Sci. Results*, *131*, 301–310.

Parés, J. M. (2004), How deformed are weakly deformed mudrocks? Insights from magnetic anisotropy, in *Magnetic Fabric: Methods and Applications*, edited by F. Martin-Fernandez et al., *Geol. Soc. Spec. Publ.*, *238*, 191–203.

Parés, J. M., B. A. van der Pluijm, and J. Dinarès-Turell (1999), Evolution of magnetic fabrics during incipient deformation of mudrocks (Pyrenees, northern Spain), *Tectonophysics*, *307*, 1–14, doi:10.1016/S0040-1951(99)00115-8.

Saito, S., M. B. Underwood, Y. Kubo, and the Expedition 322 Scientists (2010), *Proceedings of the Integrated Ocean Drilling Program*, vol. 322, Integr. Ocean Drill. Program Manage. Int., Inc., Washington, D. C., doi:10.2204/iodp.proc.322.2010.

Schwehr, K., and L. Tauxe (2003), Characterization of soft-sediment deformation: Detection of cryptoslumps using magnetic methods, *Geology*, *31*, 203–206, doi:10.1130/0091-7613(2003)031<0203:COSSDD>2.0.CO;2.

Screaton, E. J., G. Kimura, D. Curewitz, and the Expedition 316 Scientists (2009), Expedition 316 summary, *Proc. Integr. Ocean Drill. Program*, *314/315/316*, 29 pp., doi:10.2204/iodp.proc.314315316.131.2009.

Strasser, M., et al. (2009), Origin and evolution of a splay fault in the Nankai accretionary prism, *Nat. Geosci.*, *2*, 648–652.

Taira, A., and N. Niitsuma (1986), Turbidite sedimentation in the Nankai Trough as interpreted from magnetic fabric, grain size, and detrital modal analyses, *Initial Rep. Deep Sea Drill. Proj.*, *87*, 611–632.

Tarling, D., and F. Hrouda (1993), *The Magnetic Anisotropy of Rocks*, 217 pp., CRC Press, Boca Raton, Fla.

Tauxe, L. (1998), *Paleomagnetic Principles and Practice*, 299 pp., Kluwer Acad., Boston, Mass.

Tobin, H. J., and M. Kinoshita (2006), Investigations of seismogenesis at the Nankai Trough, Japan, *Integr. Ocean Drill. Program Sci. Prosp., NanTroSEIZE Stage 1*, Integr. Ocean Drill. Program Manage. Int., Inc., Washington, D. C., doi:10.2204/iodp.sp.nantroseize1.2006.

Ujiie, K., T. Hisamitsu, and A. Taira (2003), Deformation and fluid pressure variation during initiation and evolution of the plate boundary decollement zone in the Nankai accretionary prism, *J. Geophys. Res.*, *108*(B8), 2398, doi:10.1029/2002JB002314.

Yoshioka, S., and K. Murakami (2007), Temperature distribution of the upper surface of the subducted Philippine Sea Plate along the Nankai Trough, southwest Japan, from a three-dimensional subduction model: Relation to large interplate and low-frequency earthquakes, *Geophys. J. Int.*, *171*, 302–315, doi:10.1111/j.1365-246X.2007.03510.x.